Available online at www.synsint.com

Synthesis and Sintering

ISSN 2564-0186 (Print), **ISSN** 2564-0194 (Online)

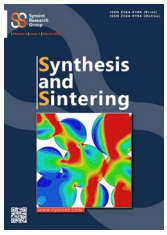

Research article

Finite element analysis of additive manufacturing-enabled cellular architectures for morphing airfoil applications

Tyou Al-Oussainne, Ata Khabaz-Aghdam *

Department of Aeronautical Engineering, Faculty of Aviation and Space Sciences, University of Kyrenia, Kyrenia, Mersin 10, Turkey

A B S T R A C T

Morphing airfoil structures require internal architectures that provide both sufficient flexibility and structural reliability while remaining compatible with advanced manufacturing techniques. In this study, the structural performance of different cellular core configurations suitable for additive manufacturing was investigated using finite element analysis. Four internal architectures were considered, including a conventional honeycomb structure (HC), a re-entrant auxetic structure (RA), and two modified auxetic configurations (CA-1 and CA-2). The airfoil models were subjected to loading conditions ranging from 50 N to 300 N to evaluate stress distribution and deformation behavior. The results demonstrate that cellular geometry significantly influences the mechanical response of the morphing airfoil. The HC configuration exhibited the highest stiffness, with the lowest displacement (2.63 mm at 300 N), but showed pronounced stress concentration. In contrast, the auxetic configurations provided more uniform stress distribution due to their geometry-driven deformation mechanisms. The CA-2 design showed the highest deformation capability, indicating enhanced flexibility and morphing potential, while also maintaining a relatively uniform stress distribution. In contrast, the RA configuration exhibited localized stress concentration associated with its re-entrant geometry. Overall, the modified auxetic configuration CA-2 demonstrated the most balanced mechanical performance by combining improved stress redistribution with high deformation capability. The results highlight that geometrically optimized auxetic structures, which can be readily fabricated using laser-based additive manufacturing techniques, offer significant potential for morphing airfoil applications.

KEYWORDS

Morphing airfoil
Cellular internal structures
Auxetic structure
Finite element analysis

OPEN ACCESS

1. Introduction

Improving aerodynamic efficiency and flight performance across a wide range of operating conditions remains a major challenge in modern aircraft design. Conventional aircraft wings are generally optimized for a single flight condition, which leads to performance compromises during off-design phases such as takeoff, climb, and landing. With increasing demands for fuel efficiency and environmental sustainability in aviation, there is a growing need for adaptive wing technologies capable of improving aerodynamic performance under varying flight conditions [1–4].

Morphing wing technology has emerged as a promising solution to address these limitations. Morphing wings can alter their shape in a controlled manner to adapt to changing aerodynamic requirements. Such adaptations may involve variations in camber, twist, span, or airfoil thickness, allowing the wing to maintain optimal aerodynamic performance across different flight regimes [1, 2, 5]. Inspired by the adaptive wing motions observed in birds, morphing aircraft structures

* Corresponding author. *E-mail address:* ata.khabazaghdam@kyrenia.edu.tr (A. Khabaz-Aghdam)
Received 2 January 2026; Received in revised form 27 March 2026; Accepted 27 March 2026.

https://doi.org/10.53063/synsint.2026.61323

have been widely investigated to improve lift-to-drag ratio, reduce drag, enhance maneuverability, and increase overall flight efficiency [1, 6].

Early morphing wing concepts relied primarily on mechanical mechanisms such as hinges, sliding joints, and discrete control surfaces. Although these mechanisms allow geometric modification of the wing structure, they often introduce structural discontinuities, additional weight, increased system complexity, and higher maintenance requirements [3, 5]. As a result, recent research has focused on the development of compliant morphing structures that enable smooth and continuous deformation without relying on traditional mechanical joints. These compliant structures rely on distributed structural flexibility to achieve shape adaptation while maintaining aerodynamic smoothness and structural integrity [7, 8].

Recent advances in additive manufacturing (AM), particularly laser-based techniques such as selective laser melting (SLM) and laser powder bed fusion (LPBF), have enabled the fabrication of complex internal architectures that were previously difficult or impossible to manufacture using conventional methods. These technologies allow the realization of intricate cellular structures with high geometric fidelity, making them highly suitable for lightweight and multifunctional aerospace components [9, 10].

Among the various structural approaches proposed for morphing applications, cellular structures have attracted significant attention due to their lightweight characteristics and tunable mechanical behavior. Cellular architectures can provide a desirable balance between stiffness and flexibility, allowing controlled structural deformation while maintaining sufficient load-bearing capacity [11]. One particular class of cellular materials that has received increasing attention is auxetic materials [12].

Auxetic materials exhibit a negative Poisson's ratio, meaning that they expand laterally when stretched and contract laterally when compressed, which is opposite to the behavior of conventional materials. This unusual mechanical response originates primarily from the internal geometry of the structure rather than the base material properties [13]. Auxetic structures demonstrate several advantageous mechanical properties, including enhanced shear resistance, improved indentation resistance, higher energy absorption capability, and superior fracture toughness [14]. Because of these characteristics, auxetic materials have been investigated for a wide range of engineering applications, including aerospace structures, impact-resistant panels, biomedical devices, and adaptive structures [15].

One of the most widely studied auxetic geometries is the re-entrant honeycomb structure. This configuration consists of inwardly inclined cell walls that rotate and unfold under applied loads, producing the negative Poisson's ratio behavior [16]. Re-entrant honeycomb structures are particularly attractive for morphing wing applications because they allow significant structural deformation while maintaining overall structural connectivity. Previous studies have demonstrated that auxetic cellular structures can significantly enhance morphing capability by enabling smooth camber variation while maintaining load transfer within the wing structure [17].

Several researchers have investigated the potential of auxetic and compliant cellular structures for aerospace applications. Alderson and his coworker [18] reviewed the development and engineering applications of auxetic materials, emphasizing their enhanced fracture resistance and energy absorption characteristics. Budarapu et al. [7] proposed a design framework for morphing airfoils incorporating auxetic cellular structures and showed that such configurations can provide improved flexibility along the chordwise direction while maintaining structural stability. Further investigations have explored compliant cellular concepts for passive morphing systems. Hou et al. [19] reported that re-entrant hexagonal honeycomb cores can exhibit high shear flexibility together with reduced stress concentration compared with conventional honeycomb designs when equivalent stiffness conditions are considered. In addition, Bettini et al. [20] investigated composite chiral cellular structures for morphing airfoil applications and showed that these architectures can achieve large overall displacements with relatively low material strain, making them attractive for adaptive aerospace structures.

Despite these advantages, conventional re-entrant auxetic geometries often suffer from high stress concentrations at sharp internal corners of the cellular ligaments. These stress concentrations can lead to structural weaknesses, reduced fatigue life, and potential failure under repeated loading conditions. Previous research has suggested that geometric modifications such as smoothing, filleting, or introducing curved ligament connections can significantly reduce stress concentrations while preserving the auxetic deformation mechanism.

However, further investigation is required to systematically evaluate how such geometric modifications influence the structural performance of auxetic cellular cores when integrated within realistic airfoil geometries. In particular, understanding the relationship between cellular geometry, stress distribution, and deformation capability is essential for the design of efficient morphing wing structures.

In this context, the present study investigates the structural performance of different cellular internal architectures embedded within an airfoil configuration for morphing wing applications. A conventional honeycomb structure is first analyzed as a reference configuration due to its well-known structural efficiency. Subsequently, a re-entrant auxetic cellular structure is introduced and compared with modified auxetic geometries incorporating curved ligament connections aimed at reducing stress concentration.

Finite element analysis is performed under multiple loading conditions to evaluate the resulting stress distribution and deformation behavior of each configuration. The results of this study are expected to provide insight into the design of lightweight and flexible cellular structures compatible with additive manufacturing, capable of improving the structural adaptability and efficiency of morphing wing systems.

2. Materials and methods

2.1. Airfoil configuration

In this study, the structural behavior of a morphing wing section was investigated using a cellular internal structure integrated within an airfoil geometry. The selected airfoil for the present analysis is the Eppler 420 airfoil, which is widely used in aerodynamic studies involving morphing and flexible wing concepts.

The Eppler 420 airfoil was chosen primarily because of its relatively high camber and favorable aerodynamic characteristics at low Reynolds numbers. These characteristics make it particularly suitable for studying camber morphing mechanisms, where the trailing edge deformation plays a critical role in modifying aerodynamic performance. In addition, this airfoil has been frequently used in previous morphing-wing investigations, allowing easier comparison with existing studies.

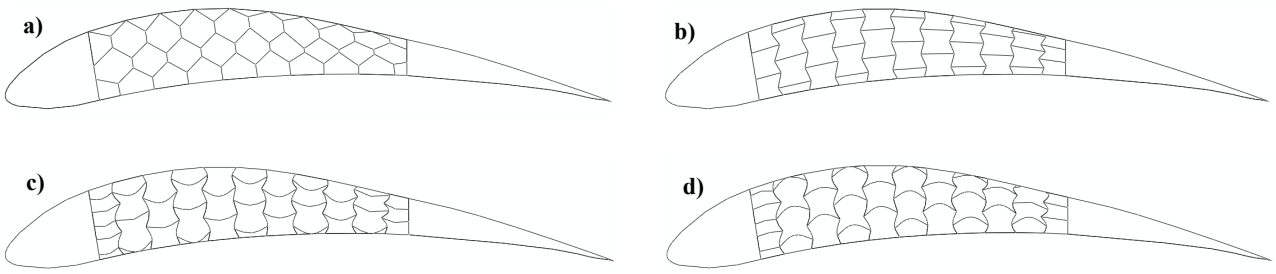

Fig. 1. Eppler 420 airfoil with different infill designs: a) conventional honeycomb structure, b) re-entrant auxetic honeycomb structure, and c, d) re-entrant auxetic structure with curved connections.

The internal structure of the airfoil was modeled using different cellular configurations to evaluate their influence on deformation capability and stress distribution. The cellular core is embedded between the upper and lower skins of the airfoil, forming a lightweight but load-bearing internal framework capable of transmitting loads while enabling structural flexibility.

2.2. Cellular infill configurations

To evaluate the influence of cellular geometry on structural performance, four different infill configurations were considered in this study. These configurations are illustrated in Fig. 1 and represent a progressive modification of conventional cellular structures toward auxetic geometries.

The first configuration corresponds to a conventional honeycomb structure, which is widely used in aerospace sandwich panels due to its excellent stiffness-to-weight ratio and efficient load distribution capability. The honeycomb geometry consists of regular hexagonal cells that provide high structural stiffness but relatively limited deformation capability. For this reason, the honeycomb structure was used as the reference configuration in this study.

The second configuration is a re-entrant auxetic honeycomb structure, which is obtained by modifying the geometry of the conventional honeycomb cells so that the cell walls are inclined inward. This geometric modification produces a negative Poisson's ratio, meaning that the structure expands laterally when stretched and contracts when compressed. Such behavior allows the structure to undergo larger and more uniform deformation, which is highly desirable in morphing wing applications.

The third and fourth configurations introduce a geometric modification to the re-entrant auxetic structure by replacing the sharp corners of the ligaments with two different curved connections. For clarity in the subsequent discussions, the investigated configurations are identified using short codes. The conventional honeycomb structure is denoted as HC, the re-entrant auxetic configuration as RA, the convex curved auxetic design as CA-1, and the concave curved auxetic configuration as CA-2.

2.3. Geometrical parameters

The overall geometry of the morphing wing section and the cellular core structure is defined using the parameters summarized in Fig. 2 and Table 1. These parameters include the airfoil chord length, distances from the leading and trailing edges used to define the internal structural layout, and the thickness of both the skin and internal cellular members.

The chord length of the airfoil was defined as 700 mm, representing the overall length of the wing section considered in the numerical model. The internal cellular framework was positioned within the airfoil using two reference distances: 110 mm from the leading edge and 235 mm from the trailing edge. These distances determine the region in which the cellular structure is distributed inside the airfoil.

The thickness of the skin layer was assigned as 2.53 mm, while the thickness of the internal cellular ligaments was set to 1 mm for all investigated configurations. Using identical geometric parameters for all models ensures that any difference in structural response can be attributed solely to the influence of cellular geometry.

The design parameters used in the numerical model are summarized in Table 1.

2.4. Material properties

All structural components of the airfoil, including the skins and cellular core structures, were modeled using aluminum 6061, which is commonly used in aerospace structures due to its favorable combination of strength, lightweight characteristics, and corrosion resistance.

The mechanical properties assigned to the material are summarized in Table 2. The density of the material was defined as 2700 kg/m^3, while the Young's modulus was taken as 68,900 MPa, representing the elastic stiffness of the aluminum alloy. A Poisson's ratio of 0.33 was used to describe the elastic deformation characteristics of the material.

In addition, the yield strength and ultimate tensile strength were defined as 276 MPa and 310 MPa, respectively. These values allow the structural response of the airfoil to be evaluated relative to the material strength limits during the numerical simulations.

Table 1. Design parameters.

Symbol	Parameter		Dimension
t_S	Skin and infill thickness	2.53	mm
t_D	Infill pattern thickness	1	mm
α	Cell internal wall angle	6	°
a	Distance from leading edge	110	mm
b	Distance from trailing edge	235	mm
c	Chord length	700	mm

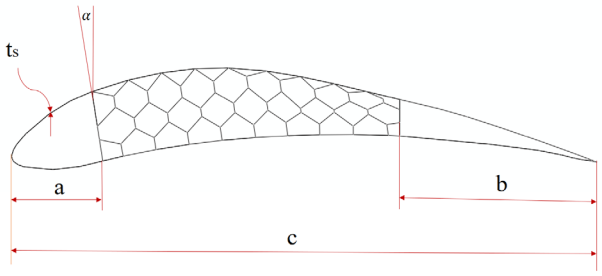

Fig. 2. Configuration and geometric parameters of the airfoil model (illustrated for the honeycomb structure as a representative case).

Using the same material properties for all configurations ensures that the comparison among different cellular structures is based solely on geometric effects rather than material differences.

2.5. Finite element modeling

The structural analysis of the airfoil with different internal cellular configurations was carried out using the finite element method implemented in ABAQUS. The numerical model was developed to evaluate the stress distribution and deformation behavior of the morphing airfoil under external loading conditions.

To efficiently represent the thin-walled structure of the airfoil skins and the internal cellular patterns, two-dimensional shell elements (S4R) were employed. Shell elements provide an accurate representation of thin structures while significantly reducing the computational cost compared to solid elements. These elements were used to model both the external airfoil skin and the internal cellular structures of the different infill configurations. The meshed models of the airfoils with various cellular architectures are illustrated in Fig. 3.

Table 2. Material property of aluminum 6061 [21].

Aluminum 6061	Value
Density (kg/m^3)	2700
Young's modulus (MPa)	68900
Poisson ratio (-)	0.33
Yield strength (MPa)	276
Ultimate strength (MPa)	310

In order to represent the geometric thickness of the airfoil in the spanwise direction, a depth of 50 mm was assigned to the airfoil model. Additionally, three-dimensional structural elements (C3D8R) were used in the trailing-edge region of the airfoil where geometric continuity and structural stability are critical. This hybrid modeling approach allowed the structural behavior of both thin-walled and localized three-dimensional regions to be captured more accurately.

A structured meshing strategy was adopted to ensure a reliable numerical solution while maintaining reasonable computational efficiency. The global element size was defined as 4 mm for the entire model. This mesh size provided a sufficient level of refinement to capture stress gradients within the cellular ligaments and the airfoil skins. The mesh density was kept consistent across all configurations so that the structural response could be directly compared without numerical bias.

For the structural analysis, appropriate boundary conditions were applied to represent the support conditions of the airfoil. The leading edge of the airfoil was fully constrained, preventing translational and rotational motion. This boundary condition simulates a fixed attachment of the airfoil to the wing structure.

External loading was applied at the upper vertex of the trailing edge, representing the aerodynamic or actuation force responsible for

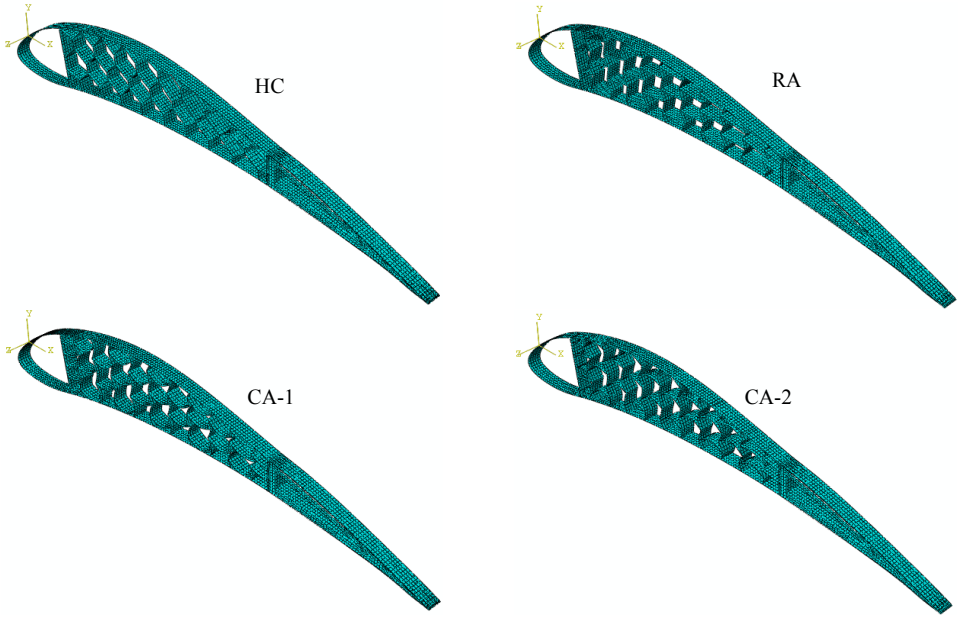

Fig. 3. Finite element mesh of the airfoil models with different internal cellular architectures (HC, RA, CA-1, and CA-2), showing the discretization of both the airfoil skin and internal lattice structures using shell elements.

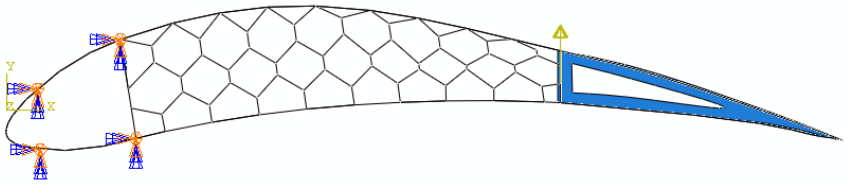

Fig. 4. Boundary conditions and loading configuration applied to the airfoil model (illustrated for the honeycomb structure as a representative case), including fully constrained leading edge and vertical load applied at the trailing edge.

inducing camber deformation in morphing wing applications. Although a concentrated point load was adopted in the present study for comparative structural evaluation, real morphing wing structures are subjected to distributed aerodynamic pressure loads. Incorporating such loading conditions will be considered in future investigations. The loading and boundary conditions applied to the reference honeycomb configuration are shown in Fig. 4, which is representative of all investigated models.

To investigate the structural response under increasing load levels, a series of static loading cases were considered, with the applied force gradually increased up to 300 N.

This modeling approach ensured consistent numerical conditions for all investigated configurations, allowing the influence of internal cellular geometry on stress distribution and deformation behavior to be systematically evaluated.

3. Results and discussion

The structural behavior of the four airfoil configurations—honeycomb (HC), re-entrant auxetic (RA), and the two modified auxetic structures (CA-1 and CA-2)—was evaluated under 300 N loads. Finite element simulations were performed to determine the stress distribution and deformation characteristics of each configuration.

The resulting Von Mises stress contours and displacement distributions are presented in Figs. 5 & 6, respectively. In addition, comparative plots derived from these data are illustrated in Fig. 7 to highlight the relationships between load, stress, and structural deformation.

3.1. Von Mises stress distribution

Fig. 5 illustrates the Von Mises stress distribution for all investigated airfoil configurations subjected to a load of 300 N applied at the trailing edge, while the leading edge is fully constrained. A clear distinction can be observed between the conventional honeycomb (HC) structure and the auxetic-based designs.

In the HC configuration, a pronounced stress concentration is formed near the upper skin of the airfoil, reaching a maximum value of approximately 153 MPa. This localized stress accumulation indicates that the load transfer occurs through limited load paths, resulting in inefficient stress redistribution within the structure.

In contrast, the auxetic configurations (RA, CA-1, and CA-2) exhibit a significantly more uniform stress distribution throughout the airfoil

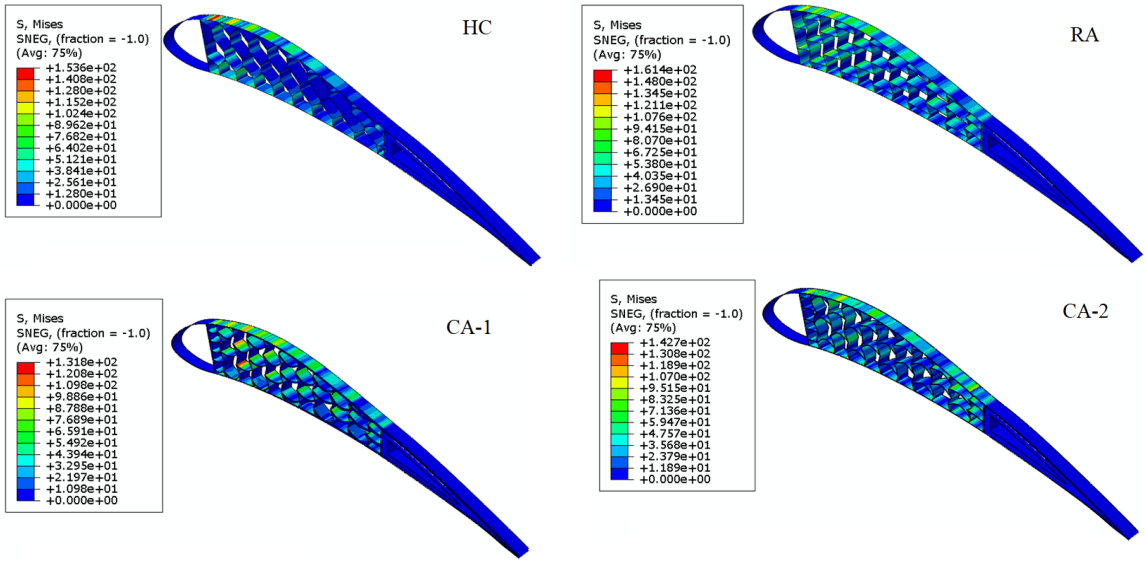

Fig. 5. Von Mises stress distribution of different airfoil configurations with various infill patterns (HC, RA, CA-1, and CA-2) under an applied load of 300 N at the trailing edge with a fully constrained leading edge.

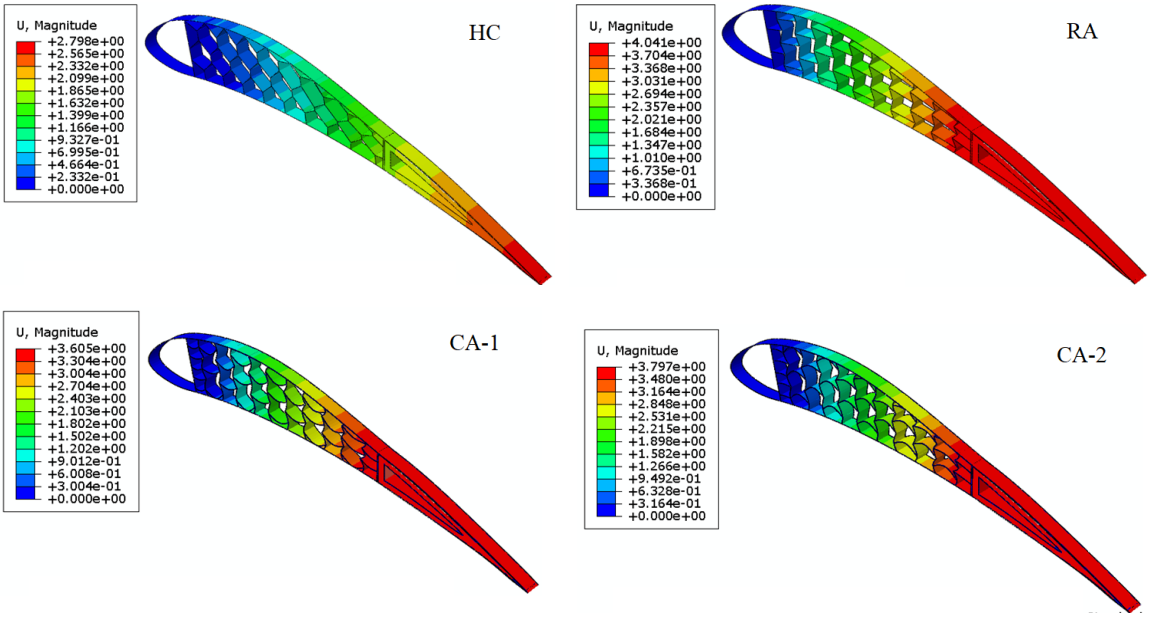

Fig. 6. Displacement distribution contours for airfoil models with different infill patterns, illustrating deformation mechanisms and strain localization behavior under loading.

body. The stress is dispersed over a larger volume, and no critical concentration zones are observed. This behavior can be attributed to the intrinsic deformation mechanisms of auxetic structures, particularly their negative Poisson's ratio, which promotes lateral expansion under loading. As a result, additional load paths are activated, enabling more effective stress delocalization.

Overall, the results demonstrate that auxetic infill patterns substantially enhance the structural integrity of the airfoil by mitigating stress concentrations, which are often the primary cause of failure initiation.

3.2. Displacement behavior

Fig. 6 presents the displacement distribution for the different infill patterns, highlighting the deformation characteristics of each configuration. The deformation is primarily concentrated near the trailing edge, where the external load is applied.

The HC structure exhibits relatively limited deformation, indicating a higher global stiffness. However, this reduced displacement is accompanied by localized displacement accumulation, particularly near the stress concentration regions identified earlier. This suggests a more brittle-like structural response, where deformation is restricted but failure risk is elevated.

On the other hand, the auxetic designs show a more distributed strain field, with deformation spreading more uniformly across the airfoil. Among them, the CA-2 configuration demonstrates the highest level of deformation, followed by RA and CA-1. This behavior reflects the enhanced flexibility of auxetic structures, which deform through geometric mechanisms such as cell rotation and expansion rather than purely material stretching.

Although auxetic configurations exhibit larger displacements compared to the HC structure, this increased deformability contributes to improved energy absorption capacity and reduces the likelihood of sudden failure.

3.3. Comparative analysis of load–stress and load–displacement relationships

Fig. 7a & b shows the variation of maximum Von Mises stress and maximum displacement as functions of the applied load for all configurations. Additionally, the relationship between maximum stress and maximum displacement is presented in Fig. 7c.

The load–stress curves (Fig. 7a) indicate that the HC structure experiences a rapid increase in stress with increasing load, confirming its susceptibility to stress concentration. In contrast, the auxetic designs exhibit a more gradual increase in stress, reflecting improved stress redistribution capabilities.

The load–displacement curves (Fig. 7b) show that the HC configuration maintains the lowest displacement values across all loading levels, indicating higher stiffness. Meanwhile, the auxetic structures display significantly larger displacements, particularly in the CA-2 model, which highlights their enhanced deformability.

The stress–displacement relationship (Fig. 7c) provides further insight into the structural response. The HC structure exhibits a steeper slope, meaning that stress increases rapidly with small increments in displacement. Conversely, the auxetic configurations show lower slopes, indicating a more progressive and controlled mechanical response.

This behavior is directly related to the deformation mechanisms of auxetic structures, where geometric transformations dominate the response, enabling efficient load redistribution and reducing stress concentration effects.

3.4. Overall structural performance

The overall structural performance of the airfoil is strongly influenced by the internal infill pattern. The conventional honeycomb structure

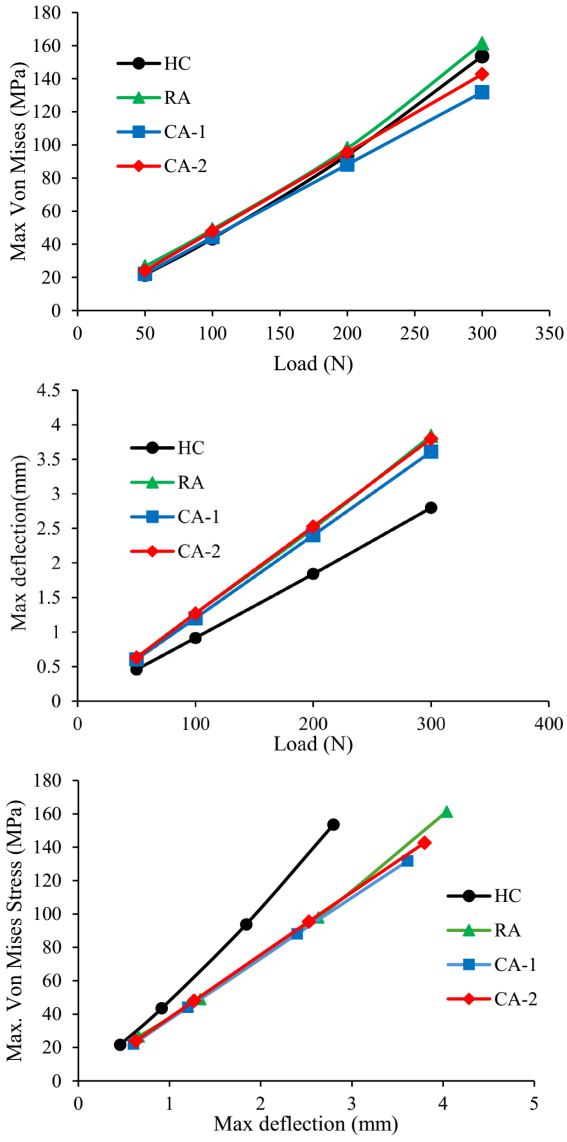

Fig. 7. a) Maximum Von Mises stress versus applied load, b) maximum displacement versus applied load, and c) maximum Von Mises stress versus maximum displacement for all investigated airfoil configurations.

offers higher stiffness and limits deformation; however, it suffers from significant stress concentration, which may lead to premature failure.

In contrast, auxetic infill patterns provide a more balanced mechanical response by combining improved stress distribution with enhanced deformation capability. The negative Poisson's ratio characteristic allows these structures to expand laterally under loading, promoting a more uniform stress field and increasing damage tolerance.

Among the investigated configurations, the CA-2 design demonstrates the most balanced mechanical performance by combining improved stress redistribution with adequate deformation capability, making it the most suitable option for morphing airfoil applications. On the other hand, the curved auxetic design (CA-2) exhibits the highest deformation capacity, indicating its potential for applications requiring energy absorption and flexibility.

In conclusion, although auxetic structures exhibit lower stiffness compared to the conventional honeycomb design, their superior ability to mitigate stress concentration, enhance load redistribution, and provide progressive deformation makes them highly promising for advanced airfoil applications, particularly under complex loading conditions.

4. Conclusions

In this study, the mechanical behavior of four different internal cellular architectures for morphing airfoil applications was systematically investigated using finite element analysis. The considered configurations included a conventional honeycomb structure (HC) as the reference design, a re-entrant auxetic structure (RA), and two modified auxetic geometries (CA-1 and CA-2). Their performance was evaluated under loading conditions ranging from 300 N, with a focus on stress distribution and deformation characteristics.

The results clearly demonstrate that the internal cellular topology plays a crucial role in governing the structural response of the airfoil. The conventional honeycomb (HC) configuration exhibited the lowest displacement under all loading conditions, confirming its relatively high stiffness. For instance, the maximum displacement of the HC structure reached only 2.63 mm at the highest load of 300 N. However, this stiffness is accompanied by pronounced stress concentration, particularly near the upper skin, which may increase the risk of localized failure.

In contrast, the auxetic configurations showed significantly improved stress distribution, characterized by a more uniform spread of stress throughout the structure. This behavior is primarily attributed to the negative Poisson's ratio and deformation mechanisms dominated by cell rotation and expansion, which promote more efficient load redistribution. Nevertheless, these advantages come at the expense of reduced stiffness, as all auxetic designs exhibited larger displacements compared to the HC configuration.

Among the auxetic structures, the CA-2 configuration exhibited the largest deformation under loading, indicating enhanced flexibility and morphing capability. However, this increased deformability was associated with relatively higher stress levels. The RA configuration also showed enhanced deformation but exhibited less efficient stress distribution compared to the modified designs, suggesting that the classical re-entrant geometry may still induce localized stress regions under certain loading conditions.

The CA-2 configuration, on the other hand, provided the most balanced mechanical performance. While its displacement remained higher than that of the HC structure, its maximum stress level was slightly lower at the highest loading condition, and the stress distribution was significantly more uniform. This indicates that the geometric modifications introduced in CA-2 effectively enhance load transfer mechanisms while maintaining adequate flexibility.

Overall, the findings suggest that although the conventional honeycomb structure offers superior stiffness, auxetic-based designs are more advantageous for morphing airfoil applications due to their enhanced deformation capability and improved stress distribution. Among the investigated configurations, the CA-2 structure presents the most favorable compromise between flexibility and structural reliability. Therefore, it can be considered a promising candidate for

advanced morphing airfoil systems where both adaptability and durability are critical requirements.

CRediT authorship contribution statement

Tyou Al-Oussainne: Software; Writing – original draft; Data curation; Investigation.
Ata Khabaz-Aghdam: Conceptualization; Methodology; Project administration; Software; Supervision; Writing – original draft; Writing– review & editing; Data curation; Investigation.

Data availability

The data underlying this article will be shared on reasonable request to the corresponding author.

Declaration of competing interest

The authors declare no competing interests.

Funding and acknowledgment

The authors would like to express their sincere appreciation to the Mechanical Engineering Department of Kyrenia University for their valuable support, cooperation, and contributions throughout the course of this study.

References

[1] S. Barbarino, O. Bilgen, R.M. Ajaj, M.I. Friswell, D.J. Inman, A Review of Morphing Aircraft, J. Intell. Mater. Syst. Struct. 22 (2011) 823–877. https://doi.org/10.1177/1045389X11414084.
[2] J. Valasek, Morphing aerospace vehicles and structures, American Institute of Aeronautics and Astronautics. (2012). https://doi.org/10.2514/4.869037.
[3] J. Sun, Q. Guan, Y. Liu, J. Leng, Morphing aircraft based on smart materials and structures: A state-of-the-art review, J. Intell. Mater. Syst. Struct. 17 (2016) 2289–312. https://doi.org/10.1177/1045389X16629569.
[4] T.A.Weisshaar, Morphing aircraft systems: historical perspectives and future challenges, J. Aircr. 50 (2013) 337–353. https://doi.org/10.2514/1.C031456.
[5] C. Thill, J. Etches, I. Bond, K. Potter, P. Weaver, Morphing skins, Aeronaut. J. 112 (2008) 117–139. https://doi.org/10.1017/S0001924000002062.
[6] B. Obradovic, K. Subbarao, Modeling of flight dynamics of morphing wing aircraft, J. Aircr. 48 (2011) 391–402. https://doi.org/10.2514/1.C000269.
[7] P.R. Budarapu, Y.B. Sudhir Sastry, R. Natarajan, Design concepts of an aircraft wing: composite and morphing airfoil with auxetic structures, Front. Struct. Civ. Eng. 4 (2016) 394–408. https://doi.org/10.1007/s11709-016-0352-z.
[8] M. Rudresh, K.P. Prashanth, P.M.V. Kumar, M. Ravikumar, S. Sivambika, Numerical investigation on flutter control of aircraft wing using auxetic structures, Res. Sq. (2025). https://doi.org/10.21203/rs.3.rs-6438799/v1.
[9] I. Gibson, D.W. Rosen, B. Stucker, Additive Manufacturing Technologies: Rapid Prototyping to Direct Digital Manufacturing, New York, NY, USA: Springer. (2015). https://doi.org/10.1007/978-1-4939-2113-3.
[10] T. DebRoy, H.L. Wei, J.S. Zuback, T. Mukherjee, J.W. Elmer, et al., Additive manufacturing of metallic components – process, structure and properties, Prog. Mater. Sci. 92 (2018) 112–224. https://doi.org/10.1016/j.pmatsci.2017.10.001.
[11] T. Li, J. Sun, J. Leng, Y. Liu, In-plane mechanical properties of a novel cellular structure for morphing applications, Compos. Struct. 305 (2023) 116482. https://doi.org/10.1016/j.compstruct.2022.116482.
[12] D. Wu, G. Yang, J. Tao, Y. Wang, H. Xiao, H. Guo, A novel cellular structure with center-symmetric cell walls for morphing applications, Compos. Struct. 352 (2025) 118644. https://doi.org/10.1016/j.compstruct.2024.118644.
[13] X. Ren, R. Das, P. Tran, T.D. Ngo, Y.M. Xie, Auxetic metamaterials and structures: a review, Smart Mater. Struct. 27 (2018) 023001. https://doi.org/10.1088/1361-665X/aaa61c.
[14] Y. Liu, C. Zhao, C. Xu, J. Ren, J. Zhong, Auxetic meta-materials and their engineering applications: a review, Eng. Res. Express. 5 (2023) 042003. https://doi.org/10.1088/2631-8695/ad0eb1.
[15] M. Mir, M.N. Ali, J. Sami, U Ansari, Review of mechanics and applications of auxetic structures, Adv. Mater. Sci. Eng. 1 (2014) 753496. https://doi.org/10.1155/2014/753496.
[16] X.T. Wang, B. Wang, X.W. Li, L. Ma, Mechanical properties of 3D re-entrant auxetic cellular structures, Int. J. Mech. Sci. 131 (2017) 396–407. https://doi.org/10.1016/j.ijmecsci.2017.05.048.
[17] Y. Zhang, W.Z. Jiang, W. Jiang, X.Y. Zhang, J. Dong, et al., Recent advances of auxetic metamaterials in smart materials and structural systems, Adv. Funct. Mater. 35 (2025) 2421746. https://doi.org/10.1002/adfm.202421746.
[18] A. Alderson, K.L. Alderson, Auxetic materials, Proc. Inst. Mech. Eng. Part G J. Aerosp. Eng. 221 (2007) 565–575. https://doi.org/10.1243/09544100JAERO185.
[19] B. Hou, A. Ono, S. Abdennadher, S. Pattofatto, Y.L. Li, H. Zhao, Impact behavior of honeycombs under combined shear-compression, Part I: Experiments, Int. J. Solids Struct. 48 (2011) 513–525. https://doi.org/10.1016/j.ijsolstr.2010.11.005.
[20] P. Bettini, A. Airoldi, G. Sala, L. Di Landro, M. Ruzzene, A. Spadoni, Composite chiral structures for morphing airfoils: Numerical analyses and development of a manufacturing process, Compos. B: Eng. 41 (2010) 133–147. https://doi.org/10.1016/j.compositesb.2009.10.005.
[21] ASM International: ASM Aerospace Specification Metals Inc. Aluminum 6061-T6; 6061-T651. Materials Park (OH): American Society of Materials. (2017).